Tribology International 177 (2023) 107973

Contents lists available at ScienceDirect

Tribology International

journal homepage: www.elsevier.com/locate/triboint

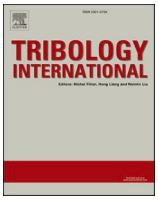

Synthesis of durable hydrophobic fluorinated polyurethanes with exceptional cavitation erosion resistance

Ning Li [a,b,1], Rui Yang [a,b,1], Ye Tian [a,b,1], Pengfei Lu [a,b], Nengliang Huang [a,b], Hua Li [a,b,c], Xiuyong Chen [a,b,c,*]

[a] Zhejiang Engineering Research Center for Biomedical Materials, Cixi Institute of Biomedical Engineering, Ningbo Institute of Materials Technology and Engineering, Chinese Academy of Sciences, Ningbo 315201, China
[b] Key Laboratory of Marine Materials and Related Technologies, Zhejiang Key Laboratory of Marine Materials and Protective Technologies, Ningbo Institute of Materials Technology and Engineering, Chinese Academy of Sciences, Ningbo 315201, China
[c] Center of Materials Science and Optoelectronics Engineering, University of Chinese Academy of Sciences, Beijing 100049, China

ARTICLE INFO

Keywords:
Fluorinated polyurethane
Synthesis
Hydrophobic
Cavitation erosion resistance

ABSTRACT

This study prepared a series of fluorinated polyurethane (FPU) with different fluorine content via changing the content of hydroxy-terminated liquid fluorine elastomer (LFH) for achieving good cavitation erosion resistance. The results showed that the FPU samples had much superior hydrophobicity, thermal stability, mechanical properties, and cavitation erosion resistance compared to the polyurethane (PU). The FPU synthesised from 20 % LFH exhibited the best properties, and its erosion rate during cavitation erosion was only 26.3 % of the PU. In addition, the simulation results suggest that the fluorine-containing soft segments in FPU were responsible for the improved properties because these soft segments would not be subjected to hydrolysis and exhibited good stability at a high temperature.

1. Introduction

Ship propellers are susceptible to cavitation erosion, corrosion, and biofouling, which result in reduced propulsion efficiency [1–5]. As the international maritime shipping consumes a considerable portion of the global transportation energy [6] and gives off a great deal of hazardous gases such as CO_2, NO_x, and SO_x [7], a slight reduction in the propulsion efficiency can lead to significant extra costs of fuel and emission of hazardous gases. Therefore, researchers have been developing coatings with effective resistance to cavitation erosion, corrosion, and fouling for decades.

Polymer and polymer-based coatings have been extensively used for corrosion-resistant and antifouling purposes [8,9]. Meanwhile, the polymer and polymer-based coatings are also very feasible to protect ship propellers due to the low cost and the simplicity for large-scale preparation. The degradation of these coatings due to the corrosion and the fouling processes is relatively slow. Nevertheless, the physical erosion can cause severe wear, compromising the corrosion-resistant and antifouling properties. For the coating applied to a propeller, the physical wear is mainly caused by cavitation erosion [2]. Hence, many studies have put great effort into developing polymer-based coatings with effective cavitation erosion resistance [10–14].

Although various polymer and polymer-based coatings have been verified their effective cavitation erosion resistance, the commercial products for resisting cavitation erosion are mainly based on polyurethane (PU), such as Belzona®– 2141 (Belzona Polymerics Ltd.). PU has high elasticity, tear resistance, dynamic mechanical properties, and good thermal stability [15,16], which are beneficial to mitigating the mechanical impact from the cavitation jets and shock waves and resisting the thermal shock during cavitation erosion. Meanwhile, PU also exhibits good wear and corrosion resistance [17,18]. However, the existence of the $–CH_2OH$ hydrophilic group on its molecular chain leads to poor water resistance, which seriously reduces the service life of PU coating [19]. The introduction of the fluorine-containing and the silicon-containing groups with low surface energy into PU can improve the hydrophobicity of PU [20–23], thereby extending its service life. Among these modified PU-based materials, most of the traditional fluorinated polyurethanes (FPU) introduce fluorine-containing groups

* Corresponding author at: Zhejiang Engineering Research Center for Biomedical Materials, Cixi Institute of Biomedical Engineering, Ningbo Institute of Materials Technology and Engineering, Chinese Academy of Sciences, Ningbo 315201, China.
E-mail address: chenxiuyong@nimte.ac.cn (X. Chen).
[1] These authors contributed equally: Ning Li, Rui Yang, Ye Tian.

https://doi.org/10.1016/j.triboint.2022.107973
Received 6 July 2022; Received in revised form 20 September 2022; Accepted 29 September 2022
Available online 3 October 2022
0301-679X/© 2022 Elsevier Ltd. All rights reserved.

in PU by end group grafting or soft chain modification [19,24–26]. However, the content of fluorine-containing small molecules introduced by these methods is limited [27], which cannot further improve the hydrophobic properties of PU.

Hydroxy-terminated liquid fluorine elastomer (LFH) has low molecular weight and good fluidity [28]. Most hydrogen atoms on the main and the side chains are replaced by fluorine, providing a material with good processing performance [29]. However, only a few kinds of LFH have been reported until now. Fluoroelastomer (VDF-co-HFP), which is copolymerised with vinylidene fluoride (VDF) and hexafluoropropylene (HFP), has excellent properties. The molecular chain contains a large number of fluorine atoms, so it has excellent hydrophobicity, heat resistance, oxidation resistance and corrosion resistance [30]. However, the application of this synthetic rubber also has some shortcomings, such as high molecular weight leading to poor processing performance and difficulty in moulding, which limit the application [30,31]. According to the reports, the VDF-co-HFP can be transformed into LFH with high fluorine content by functional group conversion technology [32]. The FPU with high fluorine content is expected to be obtained by using this fluorinated diol instead of some soft segments in the synthesis process of PU.

In this study, a series of FPU samples with different fluorine content were prepared by using 4,4-diphenylmethane diisocyanate (MDI) as the hard segment and LFH and poly-tetrahydrofuran glycol (PTMG) as the soft segment. The effects of fluorine content on the hydrophobicity and water repellency of the FPU in deionised water (DW) and artificial seawater (ASW) were studied. Meanwhile, considering the high local temperature at the cavitation erosion site [33] and the repeated impacts of micro-jets or shock waves [34], the effect of fluorine content on the thermal stability and mechanical properties of the FPU was also investigated. Finally, the cavitation erosion resistance of PU/FPU in DW was evaluated.

2. Materials and experiments

2.1. Materials

The preparation of the LFH was reported in this work [35]. LFH, poly-tetrahydrofuran glycol (PTMG, Mn=1000) and 4,4-diphenylmethane diisocyanate (MDI) were used as the raw materials for the synthesis of polyurethanes. Ethyl acetate (EA), N, N-dimethylformamide (DMF), and PTMG were purchased from Shanghai Aladdin Biochemical Technology (China). MDI was supplied by Alfa Aesar Chemical (China). The above solvents were dried through a molecular sieve (4 A, 2–3 mm, Shanghai Aladdin Biochemical Technology, China). Dibutyltin dilaurate (DBTDL), as catalysts, was supplied by Sinopharm Chemical Reagent (China). The substrate material for the coatings was 316 L stainless steel (316 L SS, Zechanglong Ltd., China).

2.2. Synthesis of the FPU

The synthesis process of the FPU was demonstrated as follows (Fig. 1). MDI was added into a 500-ml three-necked reaction flask provided with a condenser tube and a stirring device in the argon atmosphere. The temperature was raised to 50 ℃ and was kept for 1 h to evaporate the water in MDI. PTMG and LFH were desiccated in a vacuum oven at 50 ℃ for 2 h. Then, the dry PTMG were dissolved into the dry EA and slowly dripped into the flask. The stirring speed of the mixture was maintained at 150 rpm for 1 h. Next, the dry EA solution with LFH was added dropwise to the flask. The stirring speed was raised to 200 rpm, and the temperature was slowly increased to 80 ℃ and was hold for 2.5 h. Finally, the reaction device was cooled to room temperature, and the light yellow PreFPU was obtained.

The prepared PreFPU was dissolved in DMF in a ratio of 1: 3. Then, the solution was directly dripped onto a clean glass surface, naturally levelled, and dried at 60 ℃. This process was repeated five times, and then an FPU-10 sample with a thickness of 0.5 mm was obtained.

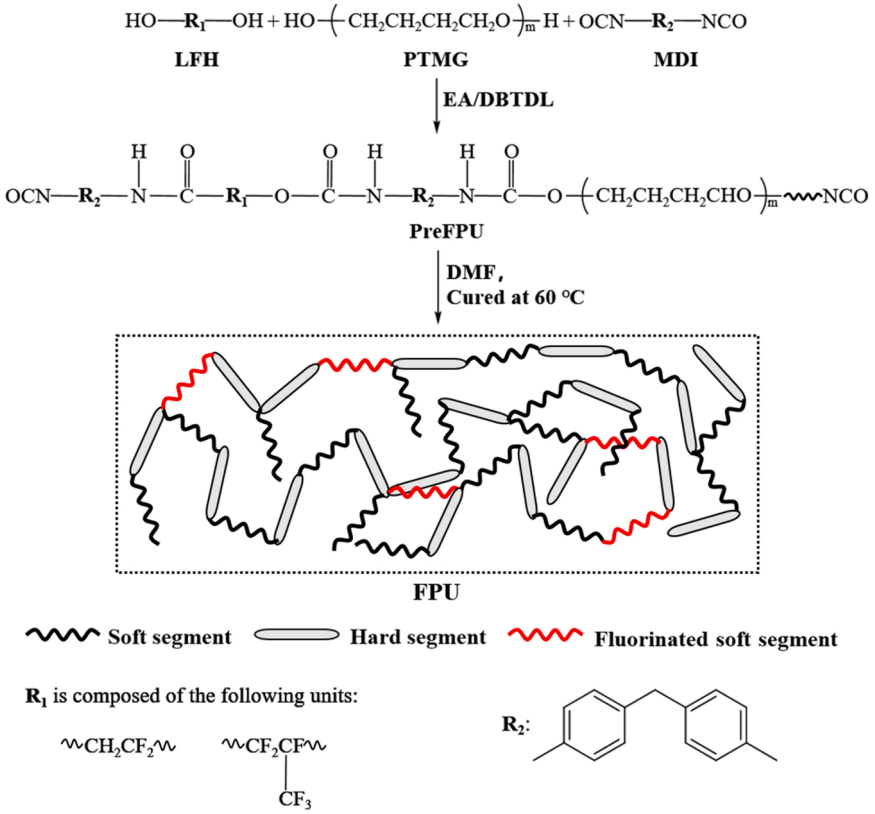

Fig. 1. Schematic diagram of the preparation process for the FPU.

Meanwhile, the other three FPU samples with different dosages of LFH were synthesised according to the formulation of materials in Table 1. The samples with the LFH content of 0, 10, 20, and 30 wt % are denoted as the PU, the FPU-10, the FPU-20, and the FPU-30, respectively.

2.3. Characterisation

Fourier transform infrared spectroscopy (ATR-FTIR) was performed using an infrared spectrometer (Nicolet iS50, Thermo Scientific, America). The spectra were recorded from 400 to 4000 cm^{-1} at a resolution of 4 cm^{-1}. X-ray diffraction (XRD) patterns of the samples were acquired by an X-ray diffractometer (D8 ADVANCE, Bruker, Germany). A copper anode was used at 40 kV and 40 mA, and the scanning range of 2θ was from 10° to 50° at a rate of 5°/min.

Water contact angle (WCA) measurement was carried out using a goniometer (DSA 25, KRUSS, Germany). The volume of the DW drop was 4 μL. Three samples were taken from each material, and each sample was tested three times. The water resistance of the polymers was characterised by the water absorption test. The samples were cut into 25 × 25 × 0.5 mm and soaked in DW and ASW, respectively. The water absorption rate (M) was calculated according to the formula below, where m_0 and m_1 are the mass of the sample before and after the soaking, respectively.

$$M = \frac{m_1 - m_0}{m_0}$$

The mechanical properties of the PU and the FPU were tested by an electronic universal testing machine (CMT500, SUST, China) according to ISO 527–2:2012. The test sample was machined into a dumbbell shape with a width of 2 mm, a span of 12 mm, a thickness of about 1 mm, and the strain rate was 30 mm/min. The glass transition temperature of the PU and the FPU was investigated via differential scanning calorimetry (DSC 214, NETZSCH, Germany), and the test temperature ranged from 100 to 200 ℃ at a heating rate of 10 ℃/min. The thermal stability of the samples was measured by a thermal gravimetric analyser (Diamond TG/DTA, PerkinElmer, America). The samples were heated from 30 to 800 ℃ at 10 ℃/min in a nitrogen ambience. The mechanical properties of the samples with respect to the temperature change were measured by a dynamic thermal mechanical analyser (DMAQ800m, TA, America). The samples were heated from − 80–100 ℃ at 10 ℃/min.

2.4. Cavitation erosion

The cavitation erosion test of the PU and the FPU was performed using an ultrasonic vibration device (GBS-SCT 20 A, Guobiao Ultrasonic Equipment Co., Ltd., Hangzhou, China) as per ASTM G32–16. Before the test, the PU and the FPU coatings were applied to 316 L SS substrates with a dimension of 20 mm in diameter and 10 mm in thickness. The coated sample was placed on a fixed bracket with a distance of 1 mm to the vibratory horn tip. During the test, the horn vibrated at a frequency of 20 ± 0.2 kHz and at a peak-to-peak amplitude of 50 μm. The mass of the sample was weighed by an electronic analytical balance (METTLER 220, TOLEDO Instruments Co., Ltd., Shanghai, China) after every test interval of 1 h, and each group of the samples was tested three times. Scanning electron microscopy (SEM, Regulus 8230, HITACHI, Japan) was used to analyse the surface morphology.

Table 1
Synthetic formulation of the FPU.

Samples	MDI (g)	LFH (g)	PTMG (g)
PU	10.8	0	20
FPU-10	10.8	3.08	16.92
FPU-20	10.8	6.16	13.84
FPU-30	10.8	9.24	10.76

2.5. Numerical simulation

The change in Gibbs free energy (ΔG) of the hydrolysis reaction at a high temperature for the PU and the FPU was calculated by the open-source software Shermo 2.3.4 [36], indicating the trend towards hydrolysis reaction for the carbamate group and the hard/soft segments. The values of the lowest unoccupied molecular orbital (LUMO) and the highest occupied molecular orbital (HOMO) of the PU and the FPU models were calculated by the open-source software Multiwfn 3.8 [37], indicating the stability of the carbamate group and the hard/soft segments in the PU and the FPU.

3. Results and discussion

3.1. ATR-FTIR analysis

The ATR-FTIR spectra of the PU and the three FPU samples are displayed in Fig. 2. All the samples exhibited the peaks at 2850 cm^{-1} and 2941 cm^{-1} identifying the asymmetrical stretching vibration caused by $–CH_3$, $–CH_2$, –CH, the peak at 1596 cm^{-1} attributed to the vibration of benzene ring skeleton [18]. The stretching vibration of N–H at 3312 cm^{-1}, the stretching vibration of C═O at 1730 cm^{-1}, the stretching vibration of C–O at 1221 cm^{-1}, and the stretching vibration of C–O–C at 1108 cm^{-1} proving the existence of –NHCOO– [38]. Meanwhile, there was no absorption peak at 2262 cm^{-1}, suggesting that –NCO group has been completely consumed [21]. For the spectra of the FPU, the absorption peaks at 880 and 1178 cm^{-1} were ascribed to the stretching vibration of C–F bond, evidencing the successful synthesis of the FPU.

3.2. XRD analysis

XRD were used to investigate the crystallinity of the PU and the FPU samples, and the XRD spectra are shown in Fig. 3. The peaks at 19.4° and 21.0° correspond to (110) and (200), respectively. The intensity of the peaks in the FPU was higher than those in the PU, suggesting the promoted crystallisation during the synthesis. The degree of crystallinity (X_c) of these samples was quantified according to the equation below [39], where A_{110}, A_{200}, and A_{ah} are the areas under the (110) peak, the (200) peak, and the amorphous halo, respectively. The results were tabulated in Table 2, showing the highest X_c was achieved by the FPU-20 sample. Since the addition of fluorine can promote the microphase separation in the molecules of FPU [40], and the microphase-separated structures can provide the space-restricted domains for crystal growths of the crystallizable blocks [41,42], the FPU showed higher X_c the PU. However, the exceeded fluorine content may inhibit the mobility of the segments due to the increased hydrogen bonds and the strengthened intermolecular interaction force [28], possibly resulting in the decreased X_c.

$$X_c = \frac{A_{110} + A_{200}}{A_{110} + A_{200} + A_{ah}}$$

3.3. Hydrophobicity and water absorption

Since it may be positively correlated to the corrosion and fouling resistance [43,44], the hydrophobicity of the PU and the FPU samples was characterised in terms of WCA, and the results were given in Fig. 4. Apart from the original samples, the WCA of the samples immersed in DW and ASW for 150 days were also measured. According to Fig. 4, the introduction of fluorine to PU could significantly change the wettability. Specifically, the increase in the fluorine content within a certain limit could result in the increase in the WCA of the samples because the enriched fluorinated alkanes on the fiber surface reduced the surface energy of the samples and hence promoted the hydrophobicity [28]. However, the exceeded fluorine content on the surface of the FPU will

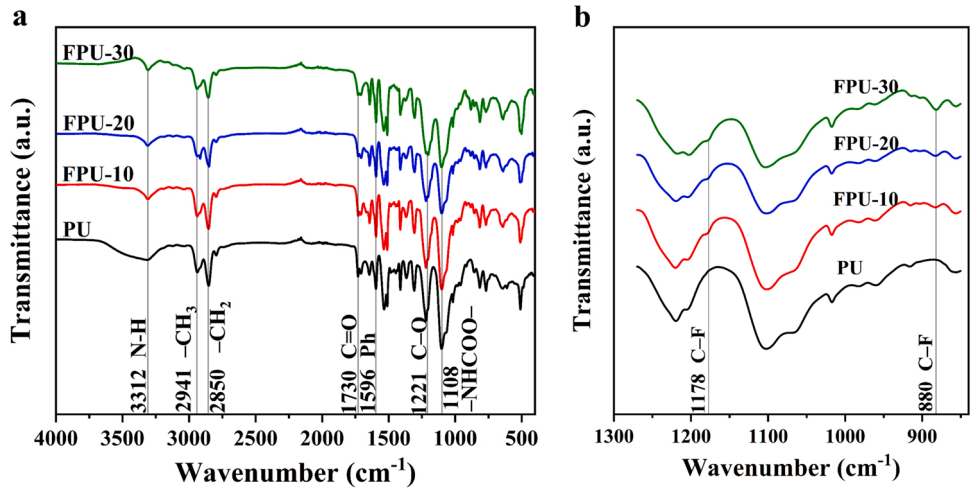

Fig. 2. The ATR-FTIR spectra of the PU, FPU-10, FPU-20, and FPU-30. a, Full scope of the spectra; **b**, Zoomed spectra showing the unique peaks in FPU.

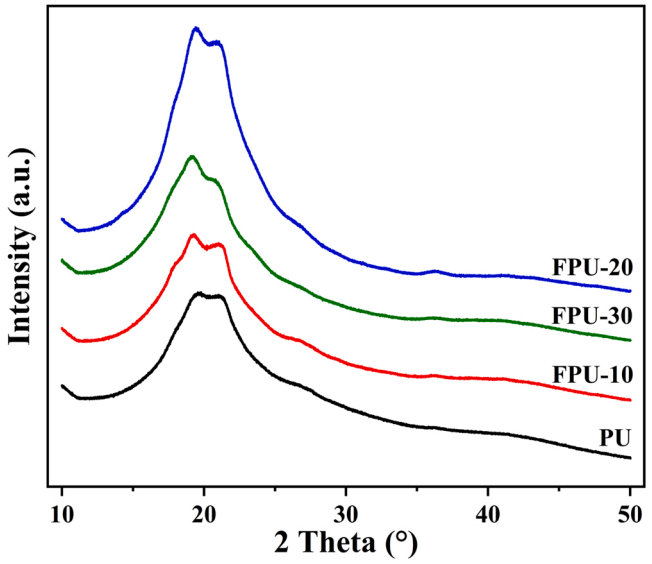

Fig. 3. The XRD spectra of the PU, FPU-10, FPU-20, and FPU-30.

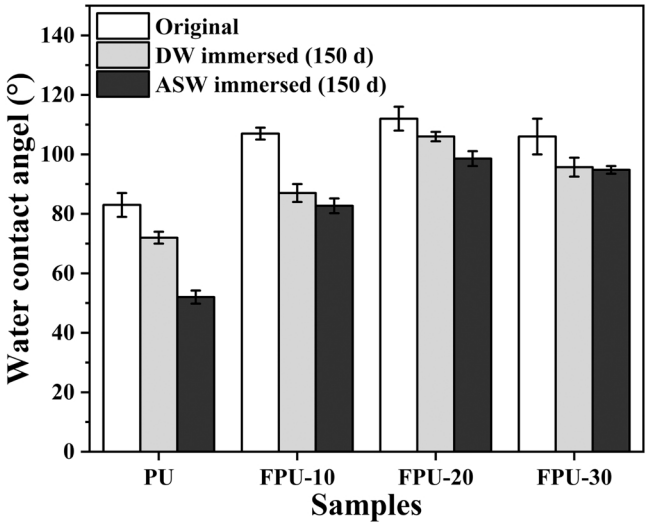

Fig. 4. The WCA of the PU and the FPU samples before and after soaked in DW and ASW.

Table 2
The degree of crystallinity of the PU and the FPU samples.

Samples	PU	FPU-10	FPU-20	FPU-30
Degree of crystallinity (%)	19.30	19.92	24.65	20.45

increase the nucleation rate and the fiber morphology on the surface of the FPU changed [45,46], which resulted in a relatively smooth surface, and thus the WCA of the FPU-30 was lower than the FPU-20. The WCA of the soaked samples was reduced but also followed the same order. Meanwhile, the WCA of the soaked FPU-20 was still greater than 100°, and the reduction was the lowest among all the samples, indicating that the FPU-20 may have good resistance to cavitation erosion even after long-time immersion in DW and ASW.

The water absorption test was performed on the PU and the FPU samples after soaked in DW and ASW for different times to further investigate whether these materials were applicable in the underwater environment for a long term, and the results are shown in Fig. 5. The water absorption of the samples gradually decreased with the extension of immersion time. This is because the PU and the FPU exhibited a network structure [21,47]. At the early stage of immersion, water molecules can quickly enter the network chain structure. However, in the later stage of immersion, water molecules in the system are almost saturated, and thus it is difficult for the subsequent water molecules to be absorbed by the samples. The results (Fig. 5) also show that the increased fluorine content could reduce the water absorption. The promoted water resistance was due to the proportion of the hydrophobic fluorine-containing groups increasing with the fluorine content, which can effectively reduce the surface energy of the materials [47]. In addition, the water absorption of samples soaked in DW (0.93 %, 0.69 %, 0.63 %, and 0.57 % for the PU, FPU-10, FPU-20, and FPU-30 samples, respectively) and ASW (1.01 %, 0.78 %, 0.73 %, 0.65 %, for the PU, FPU-10, FPU-20, and FPU-30 samples, respectively) was similar, but that of the samples soaked in ASW was slightly greater. This may be due to the corrosive ions in ASW entering into the polymers, resulting in a slight decrease in the water resistance of the samples. Therefore, the introduction of fluorine can effectively improve the water resistance of the PU, which provides the possibility for the long-term underwater application.

3.4. Thermal stability

Bubble collapse during cavitation erosion can produce instantaneous

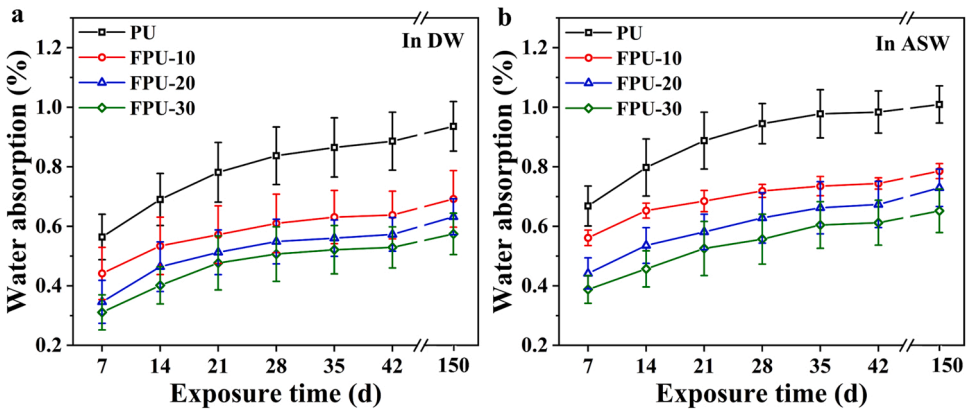

Fig. 5. Water absorption over time for the PU and the FPU. a, Soaked in DW; b, Soaked in ASW.

high temperature [33]. Thermal energy cannot be released effectively from the impact site during cavitation erosion due to the low thermal conductivity of polymers, resulting in the temperature increase at the impacted site [13]. Since the mechanical properties of the polymers are susceptible to the temperature change and are usually negatively correlated to the increased temperature, it is necessary to investigate the thermal stability of the polymers.

Thermal gravimetric analysis (TGA) is an important approach to studying the thermal stability of polymers [48], and the TGA results of the PU and the FPU samples are presented in Fig. 6, where T_5 and T_{10} denote the temperature when the polymer loses 5 % and 10 % of its initial weight, respectively. The values of the T_5, the T_{10}, and the carbon residue yields (Y_c) at 800 ℃ of the FPU samples were tabulated in Table 3. It was found that the introduction of fluorine enhanced the thermal stability of the PU. This is because the fluorine atoms with stronger electronegativity and bond energy could protect the carbon structure of the polymer [28]. However, the decreased portion of the PTMG with the increased LFH content during the synthesis process could decrease the thermal stability of the FPU [49]. As a result, the T_5 and the T_{10} of the FPU-30 were less than the FPU-20, and the most optimised LFH content to provide the best thermal stability was 20 %.

Differential scanning calorimetry (DSC) is used to evaluate the thermal transition behaviours of polymer, and it is important to investigate the glass transition temperature (T_g) and the melting point (T_m) of the FPU [50]. The DSC curves of the PU and the FPU samples were given in Fig. 7 and Table 3. The T_g of the samples increased with the increased

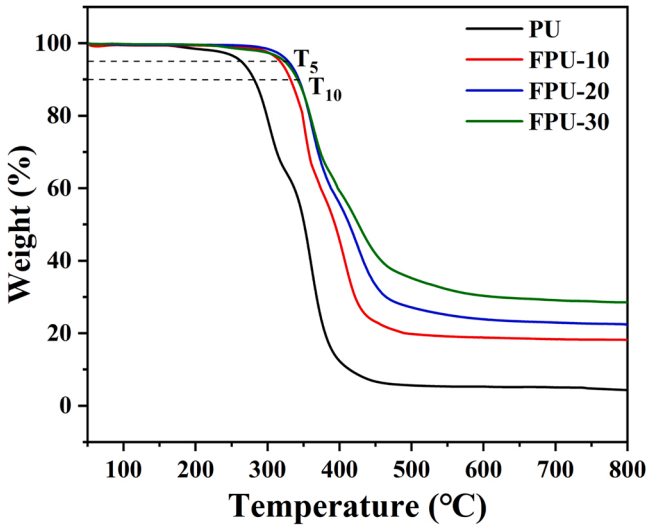

Fig. 6. TGA curves of the PU and the FPU samples.

Table 3
Thermal properties of the PU and the FPU samples.

Samples	T_5 (℃)	T_{10} (℃)	Y_c at 800 ℃, %	T_g (℃)	T_m (℃)
PU	265.5	279.3	3.96	-51.3	93.2
FPU-10	317.6	331.9	18.22	-49.7	143.0
FPU-20	328.9	343.4	22.06	-43.9	157.3
FPU-30	324.0	341.8	28.56	-40.2	135.1

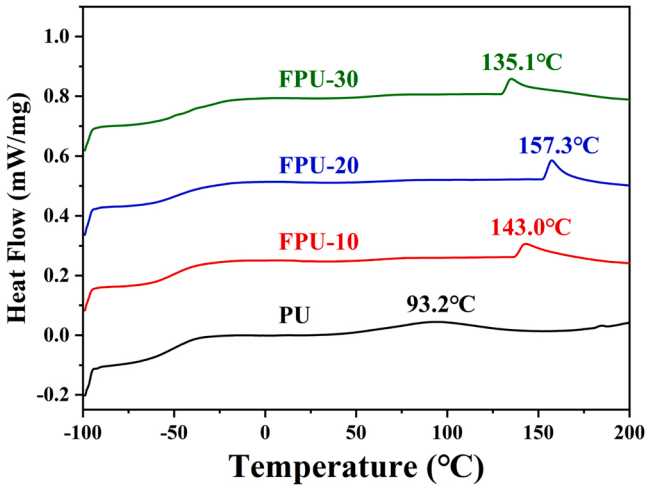

Fig. 7. DSC curves of the PU and the FPU samples.

fluorine content. This is because the LFH was introduced into the PU as a second soft segment, resulting in a cross-linking effect, and the thermal movements of the FPU chain segments were restricted [51]. Meanwhile, the melting peak of the FPU was very sharp, while that of the PU was not obvious (Fig. 7). Furthermore, the T_m of the FPU was greater than the PU. This is attributed to the introduction of fluorine increases the number of H···F hydrogen bonds, which make the ΔH larger [28]. According to the formula: $T_m = \Delta H/\Delta S$, T_m becomes larger [52]. Meanwhile, the FPU-20 had the highest T_m. The results of the TGA and the DSC tests were also in agreement with the X_c of the samples (Table 2), showing that the thermal stability of the FPU was positively correlated to the X_c.

Dynamic mechanical thermal analysis (DMTA) is an important method for evaluating the viscoelastic behaviour of polymers [53]. The storage modulus and the dissipation factor (Tan δ) with respect to the temperature for the PU and the FPU samples are shown in Fig. 8. Obviously, the storage modulus of the FPU was above 10^3 MPa between − 80 and − 60 ℃ (Fig. 8a). This is because there is no stress relaxation

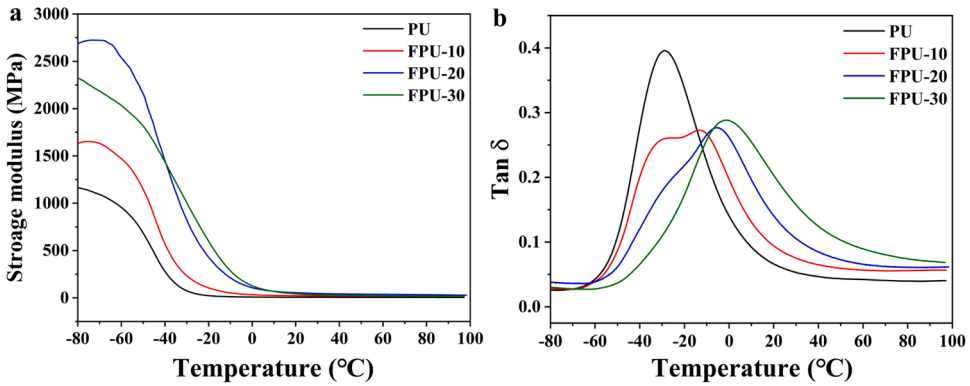

Fig. 8. Dynamic mechanical thermal analysis (DMTA) of the PU and the FPU samples. a, Storage modulus; **b**, Tan δ.

due to the temperature below T_g, and thus flexible chain could not move freely [28,54]. Moreover, the storage modulus increased with the introduction of fluorine and was raised significantly with the increase of the LFH content, since the introduction of the fluorine could increase the number of the hydrogen bonds in the PU, enhancing the intermolecular forces [28]. Hence, the FPU possessed excellent elasticity and can decrease the damage of energy impact to the substrate. As shown in Fig. 8b, the Tan δ of the FPU-10, the FPU-20, and the FPU-30 was smaller than the PU. Generally, the value of Tan δ represents the viscoelastic property of the material [21,55]. Tan δ is positively correlated with the viscosity of the material and negatively correlated with the elasticity of the material. Therefore, the FPU samples had lower viscosity and higher elasticity compared to the PU, which would give them excellent impact resistance.

3.5. Mechanical properties

The mechanical properties of the materials were investigated since they can be corrected to the cavitation erosion performance [17,34]. The tensile test was performed on the PU and the FPU samples, and the results are given in Fig. 9**a** and Table 4. The ultimate tensile strain (ε_{UT}) of the PU was 932 %, but the ε_{UT} of the FPU reduced and continuously decreased with the increase of the fluorine content (Fig. 9**a** and Table 4). However, the FPU-20 exhibited the best ultimate tensile strength (σ_{UT}) and elastic modulus (E). This could be attributed to the high X_c of the FPU-20 (Table 2) because the mechanical properties of polymers can be positively correlated to X_c [56]. Meanwhile, the fracture energy (W) of the FPU-20 was also the greatest (Fig. 9**d**).

Considering the long-term use of the material, the mechanical properties of the polymers immersed in DW and ASW for 30 days were also studied, and the results are given in Fig. 9b-c and Table 4. Generally, the σ_{UT} and the ε_{UT} of the samples decreased when the samples were

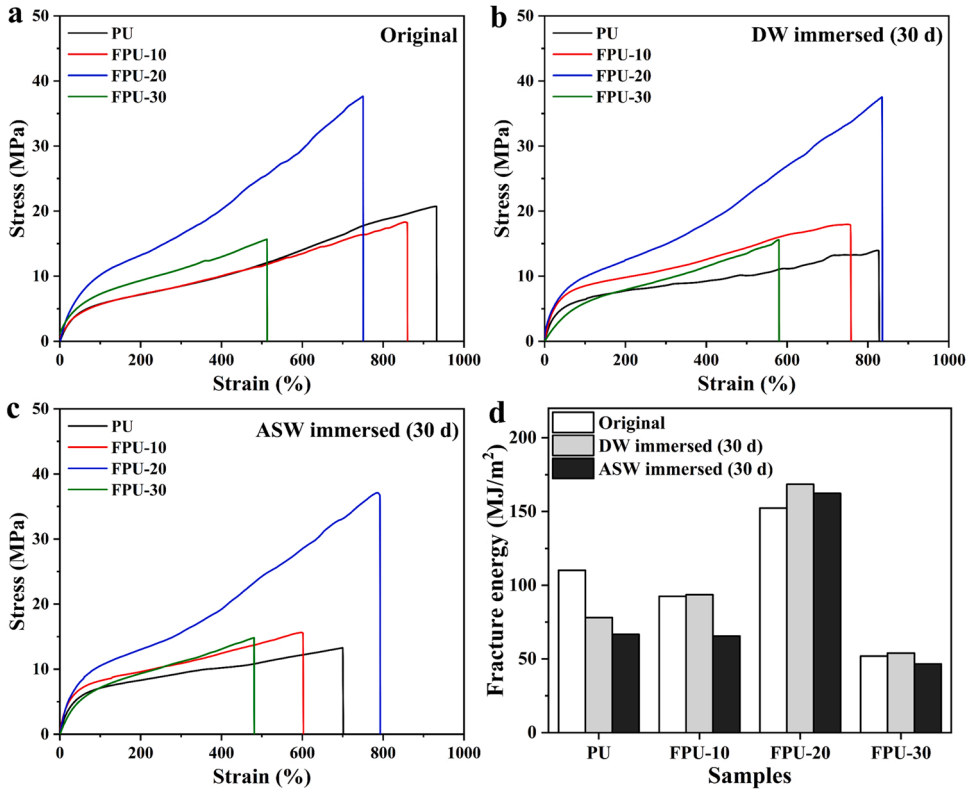

Fig. 9. Stress-strain curves and fracture energy of the PU and the FPU. a-c, The stress-strain curves of the original samples, the samples soaked in DW for 30 days, and the samples soaked in ASW for 30 days, respectively; d, The fracture energy of the materials.

Table 4
Mechanic properties the PU and the FPU.

Samples		σ_{UT} (MPa)	ε_{UT} (%)	E (MPa)	W (MJ/m^2)
Original	**PU**	20.75	932	1.55	110
	FPU-10	18.32	864	1.49	93
	FPU-20	37.64	750	3.58	152
	FPU-30	15.68	522	2.80	52
Immersed in DW for 30 days	**PU**	13.96	834	1.68	78
	FPU-10	17.97	770	2.11	94
	FPU-20	37.54	835	3.20	168
	FPU-30	13.24	519	2.13	54
Immersed in ASW for 30 days	**PU**	13.28	709	2.79	67
	FPU-10	15.64	633	2.89	66
	FPU-20	37.10	792	3.28	162
	FPU-30	13.34	478	2.29	47

immersed in DW and ASW, and the decrement was greater in the ASW than in the DW. However, the E of the DW-immersed and the ASW-immersed materials increased. Nevertheless, the FPU-20 was an exception. The σ_{UT} and the E were barely changed, and the ε_{UT} increased for the DW-immersed and the ASW-immersed FPU-20 samples. Furthermore, the W of the immersed FPU-20 was still the greatest among all the samples and increased regardless of the immersion medium. The above results suggest that the introduction of fluorine with a proper content to PU may effectively improve the service life.

3.6. Cavitation erosion performance

The cumulative mass loss and the mass loss rate with respect to the test time of the PU and the FPU coatings subjected to cavitation erosion are shown in Fig. 10. The total mass loss after cavitation erosion for 10 h and the average erosion rate from the 8th to the 10th hour are summarised in Fig. 11. According to Fig. 10b, the PU and the FPU coatings had no obvious incubation period, and the mass loss rate increased first and then decreased. The large initial cavitation erosion rate of polymers was also reported in other studies [10,14,21]. For the PU/FPU prepared in this work, the large initial cavitation erosion rate was possibly attributed to the removal of some residual unreacted small molecules or impurities on the surface of the PU/FPU due to the repeated cavitation impacts. After 4 h, the mass loss rate of the coatings gradually decreased

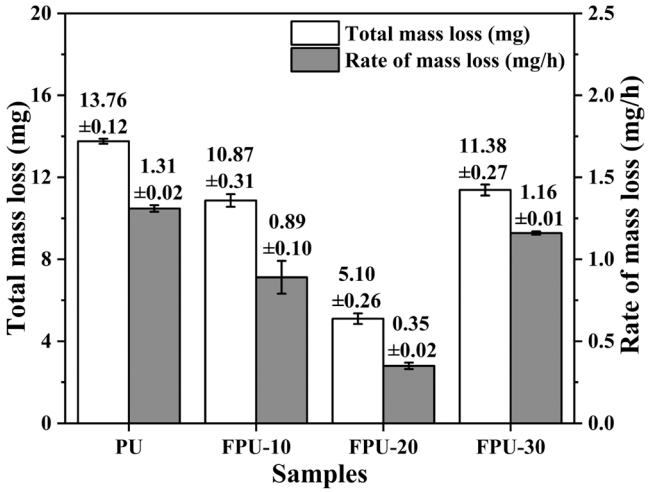

Fig. 11. Total mass loss after exposure to cavitation erosion for 10 h and the erosion rate from the 8th to the 10th hour for the PU and the FPU coatings. a, Total mass loss; **b**, Erosion rate.

and tended to be stable (approximately at the 8th h) with the extension of cavitation erosion time. The erosion rate of the FPU coatings also followed the same pattern as the PU coating, but the FPU coatings exhibited better cavitation erosion resistance. In addition, the FPU-20 coating exhibited the lowest total mass loss and erosion rate (Fig. 11), which were 36.7 % and 26.3 % of those of the PU coating, respectively. The improved cavitation erosion resistance of the FPU coatings suggested that the introduction of the fluorine with a proper content could significantly promote the cavitation erosion resistance of the PU coating.

The SEM images of the surface of the undamaged coatings (original) and the coatings subjected to cavitation erosion for 10 h are shown in Fig. 12 to further study the changes in surface morphology of the coating after cavitation erosion. The surface of the original PU, FPU-10, and FPU-20 coatings are very smooth and flat (**Fig. 12a1**, **b1**, and **d1**), while the surface of the FPU-20 coating exhibited many small bumps (**Fig. 12c1**). After 10 h cavitation erosion, many small cracks formed at the surface of the PU coating (Fig. 12**a**). The eroded surface of the FPU-30 coating also exhibited many small cracks, but there were also many cavitation erosion craters along these cracks (Fig. 12**d**). On the other hand, the FPU-10 coating exposed to cavitation erosion had much fewer cracks than the PU and the FPU-30 coating and only had some craters along the cracks (Fig. 12**b**). Surprisingly, the surface of the FPU-20 coating remained almost intact, suggesting its excellent cavitation resistance (Fig. 12**c**).

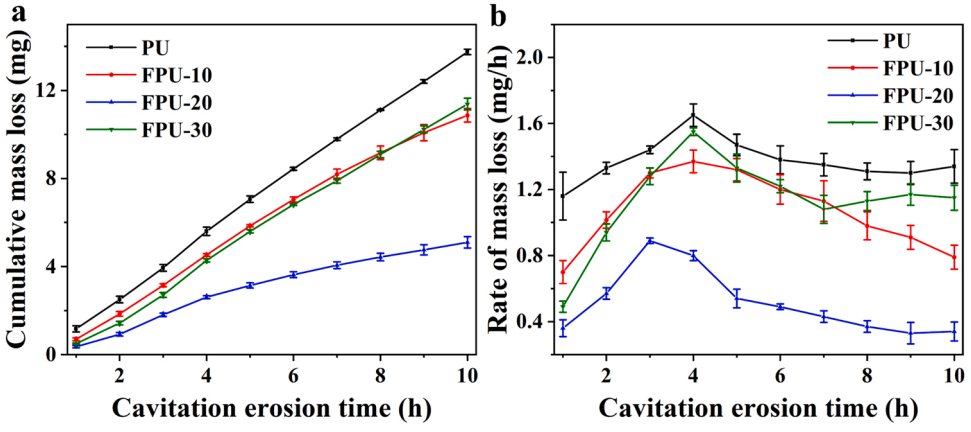

Fig. 10. Cavitation erosion results of the PU and the FPU coatings. a, Cumulative mass loss; **b**, Mass loss rate.

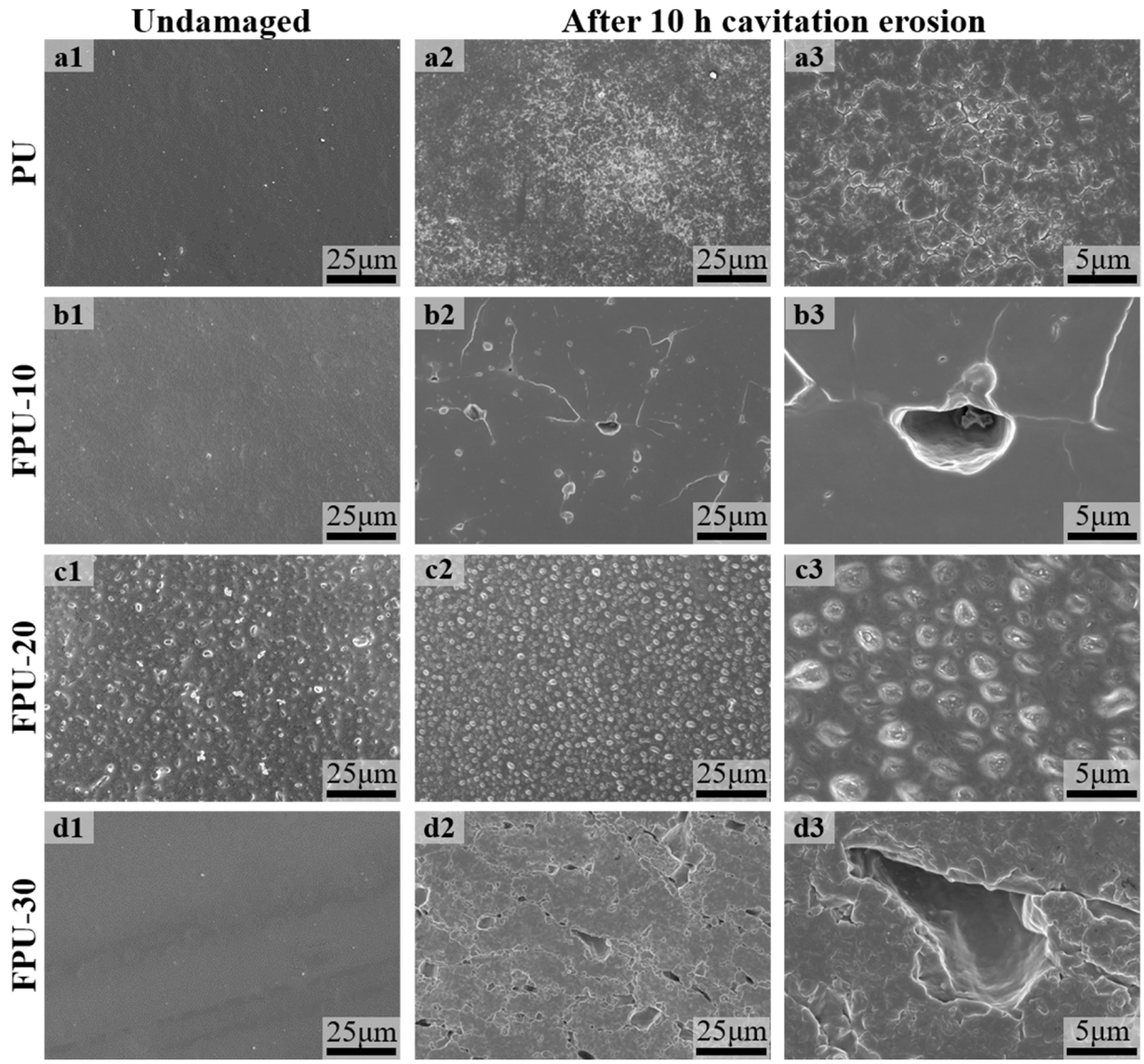

Fig. 12. SEM images of the surface of the PU and the FPU coatings before and after the exposure to cavitation erosion for 10 h.

3.7. Hydrolysis resistance, thermal stability, and mechanical properties on cavitation erosion resistance

The intense thermal energy released from the collapse of a cavitation bubble can cause the increased temperature of polymers during cavitation erosion since polymers cannot effectively dissipate the heat [13,57]. Temperature rise can result in structural changes or disaggregation of the polymers with low thermal stability, causing the compromised mechanical properties and leading to fracture during cavitation erosion [14]. In this presented study, the ether bond in the PTMG soft segment of the PU and the carbamate group can be hydrolysed at a high temperature [58]. Therefore, numerical simulations were conducted to investigate the hydrolysis reaction in the PU and the FPU.

The PU and the FPU models were simplified as OCN-Ph-CH_2-Ph-NHCOO-$(CH_2)_4$-O-$(CH_2)_4$-OH and OCN-Ph-CH_2-Ph-NHCOO-CH_2-CF_2-CF_2-CF(CF_3)-OH, respectively. The PTMG soft segment and the fluorine-containing soft segment were simplified as HO-$(CH_2)_4$-O-$(CH_2)_4$-OH and HO-CH_2-CF_2-CF_2-CF(CF_3)-OH, respectively, to save the computational cost. Hence, the expected reactions for simulation are given in **Formula 1–3**. Since the local temperature upon the collapse of cavitation bubbles can reach hundreds of degrees Celsius, these reactions were simulated at 200 °C by the open-source software Shermo 2.3.4 to calculate ΔG of each reaction. Meanwhile, the LUMO and the HOMO values of the PU and the FPU models were calculated by the open-source software Multiwfn 3.8 (Fig. 13).

According to Table 5, the values of ΔG for **Formula 1–3** were − 28.82 kJ/mol, − 41.11 kJ/mol, and − 48.44 kJ/mol, respectively. The negative values of ΔG indicated that the ether bonds in the carbamate group and the soft segment tended to be hydrolysed at a high temperature. The frontier molecular orbital theory suggests that the nucleophile (i.e., the water molecules) at HOMO can interact with the electrophile (i.e., the carbon atoms in the carbamate group) at LUMO, which results in the reaction (i.e., the hydrolysis of PU). The simulation results by Multiwfn 3.8 show that the LUMO values of the carbamate group in the PU and the FPU were 0.63 eV and 0.61 eV, respectively, suggesting that the chemical reactivity of the carbamate group in the PU and the FPU during hydrolysis was similar. Meanwhile, the hard segments of the PU and the FPU also exhibited similar HOMO-LUMO gap values (Table 6). For similar structures, a low HOMO-LUMO gap value means high stability [59,60]. Hence, the hard segments in FPU may be slightly more stable than the hard segments PU.

According to the simulation results above, the chemical reactivity of the hydrolysis of the carbamate group was expected to behave similarly in the PU and the FPU, and the stability of hard segments of the PU and

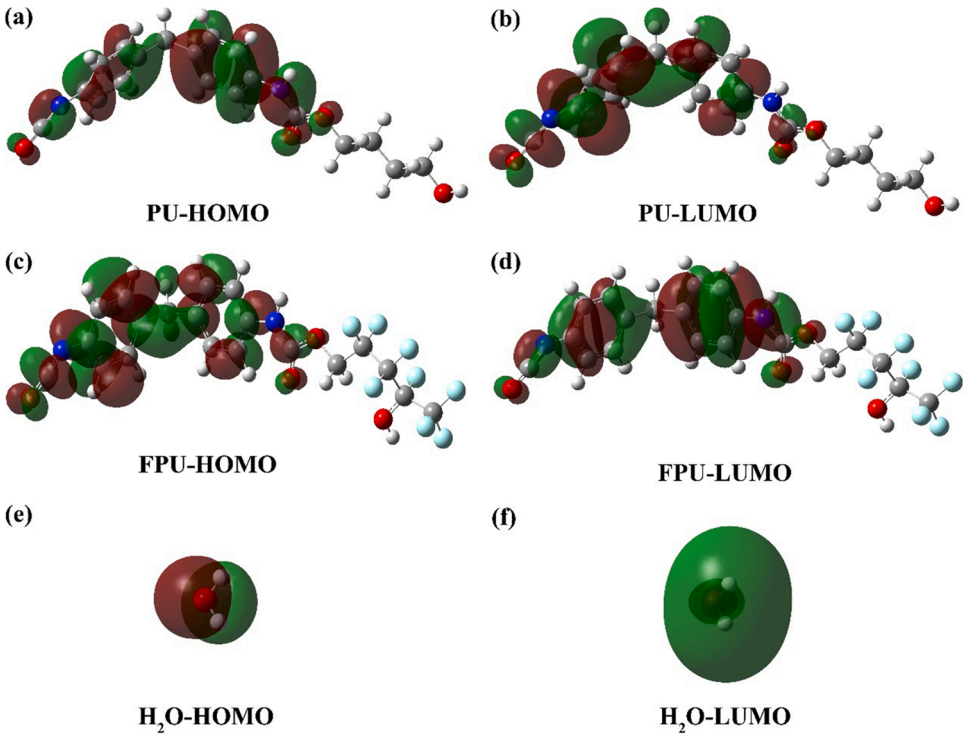

Fig. 13. Schematics showing the HOMO and LUMO of the PU/FPU (based on the simplified models) and water.

Table 5
The Gibbs free energy (G) of the related chemicals (for the simplified models of PU and FPU) at 200 °C calculated by Shermo 2.3.4.

Samples	G (kJ/mol)
OCN-Ph-CH_2-Ph-NHCOO-$(CH_2)_4$-OH	-3001763.54
H_2O	-200212.66
OCN-Ph-CH_2-Ph-NHCOOH	-2393310.48
HO-$(CH_2)_4$-O-$(CH_2)_4$-OH	-1417135.31
HO-$(CH_2)_4$-OH	-808694.54
OCN-Ph-CH_2-Ph-NHCOO-CH_2-CF_2-CF_2-CF(CF_3)-OH	-5185613.34
HO-CH_2-CF_2-CF_2-CF(CF_3)-OH	-2992563.96

Table 6
The HOMO and LUMO values of the PU/FPU (based on the simplified models) and water.

Samples	HOMO (eV)	LUMO (eV)	HOMO-LUMO gaps (eV)
Hard segment (PU)	-6.93	0.63	7.56
Hard segment (FPU)	-6.98	0.61	7.59
Soft segment (PU)	-8.86	2.33	11.19
Soft segment (FPU)	-10.175	2.17	12.34
H_2O	-10.91	2.29	13.20

the FPU may not exhibited a significant difference. Hence, it can be confirmed that the difference between the PU and the FPU in the soft segment resulted in the difference in cavitation erosion behaviour. The intense thermal energy by cavitation can cause hydrolysis of the soft segment in the PU (**Formula 2**), resulting in disaggregation. Hence, the mechanical properties of the PU can be compromised, resulting in poor resistance to cavitation erosion. However, the fluorine-containing soft segment cannot undergo hydrolysis due to the absence of the ether bond. On the other hand, as the HOMO-LUMO gap value of the fluorine-containing soft segment in FPU was lower than that of the soft segment in PU (Table 6), the fluorine-containing soft segment in FPU was much more stable than the soft segment in PU.

Since 10–30 % of the original soft segment with PTMG was replaced by the fluorine-containing soft segment segments in the FPU, the simulation results indicated that FPU was more resistant to hydrolysis. Meanwhile, the simulation results agree with the experimental results that the introduction of F improved the thermal stability of PU because the strong electronegativity, high bond energy, and shorter atomic radius of the F atoms can protect the carbon framework of the FPU [28]. Specifically, the T_m, T_5, and T_{10} of the FPU were much higher than those of the PU (Table 3). In addition, the DMTA result also indicated that the FPU might keep the mechanical properties at a high temperature (Fig. 8.). Hence, the FPU showed better cavitation erosion resistance than the original PU.

OCN-Ph-CH_2-Ph-NHCOO-$(CH_2)_4$-OH + H_2O → OCN-Ph-CH_2-Ph-NHCOOH + HO-$(CH_2)_4$-OH (1)

HO-$(CH_2)_4$-O-$(CH_2)_4$-OH + H_2O → 2 HO-$(CH_2)_4$-OH (2)

OCN-Ph-CH_2-Ph-NHCOO-CH_2-CF_2-CF_2-CF(CF_3)-OH + H_2O → OCN-Ph-CH_2-Ph-NHCOOH + HO-CH_2-CF_2-CF_2-CF(CF_3)-OH (3)

On the other hand, the differences in the cavitation erosion resistance of the FPU with different content of F could be attributed to the different mechanical properties. According to Fig. 9**d**, the fracture energy of the original FPU followed an ascending order of the FPU-20, the FPU-10, and the FPU-30, which was in agreement with the cavitation erosion test results given in Fig. 11. As the energy generated during cavitation erosion was absorbed and converted into deformation [61], higher fracture energy meant more cavitation energy was needed to cause erosion. Therefore, the fracture energy may be positively correlated to the cavitation erosion resistance of the FPU samples. However, the PU sample had the greater fracture energy than the FPU-10 and the FPU-30 samples, but its cavitation erosion resistance was inferior. However, the cavitation erosion resistance of the FPU was more dominated by the fracture energy as the thermal stability of the FPU was similar. In addition, other mechanical properties may be correlated to the behaviour of the FPU in response to cavitation impact. According to Table 4, the FPU-30 exhibited the lowest ε_{UT} and the second-highest E. Therefore, the eroded surface of the FPU-30 looked much more 'brittle'

compared to the eroded surface of other samples (Fig. 12).

4. Conclusions

Various fluorinated polyurethane (FPU) with different fluorine contents were successfully prepared by altering the dosage of the hydroxy-terminated liquid fluorine elastomer (LFH) during the synthesis process. The introduction of fluorine to the polyurethane (PU) reduced the surface energy, and thus the FPU showed good hydrophobicity. Meanwhile, as the degree of crystallinity increased, the FPU also exhibited much better thermal stability and mechanical properties compared to the PU. Therefore, the cavitation erosion resistance of these FPU samples was also promoted, and the FPU synthesised from the 20 % LFH was the best. Furthermore, the simulation results suggest that the fluorine-containing soft segments in FPU were responsible for the improved properties because these soft segments would not be subjected to hydrolysis and exhibited good stability at a high temperature. In addition, the tests on the FPU samples immersed in deionised water and artificial seawater showed that the hydrophobicity and the mechanical properties were only slightly compromised, suggesting that the FPU had the capability for long-term underwater service.

Declaration of Competing Interest

The authors declare that they have no known competing financial interests or personal relationships that could have appeared to influence the work reported in this paper.

Data Availability

Data will be made available on request.

Acknowledgments

This work was supported by the Zhejiang Provincial Natural Science Foundation of China (grant # LZ22E090001), Ningbo 3315 Talents Program (grant # 2020A-29-G), and Ningbo Science and Technology Innovation 2025 Major Program (grant # 2020Z086).

Statement of originality

The authors assure that the contents of this contribution are original, and this paper has not been submitted to any other journal for publication, or not published before elsewhere, and this article contains no libelous or unlawful statements, and does not infringe on the rights of others.

References

[1] Wittekind D, Schuster M. Propeller cavitation noise and background noise in the sea. Ocean Eng 2016;120:116–21. https://doi.org/10.1016/j.oceaneng.2015.12.060.
[2] Zhang CH, Lu F, Lu LZ. High-speed visualization of cavitation evolution around a marine propeller. J Vis (Tokyo) 2019;22(2):273–81. https://doi.org/10.1007/s12650-018-00540-7.
[3] Liang L, Pang YX, Tang Y, Zhang H, Liu H, Liu Y. Combined wear of slurry erosion, cavitation erosion, and corrosion on the simulated ship surface. 1687814019834450 Adv Mech Eng 2019;11(3). https://doi.org/10.1177/1687814019834450.
[4] Otani M, Oumi T, Uwai S, Hanyuda T, Prabowo RE, Yamaguchi T, et al. Occurrence and diversity of barnacles on international ships visiting Osaka Bay, Japan, and the risk of their introduction. Biofouling 2007;23(4):277–86. https://doi.org/10.1080/08927010701315089.
[5] Song S, Demirel YK, Atlar M. Penalty of hull and propeller fouling on ship self-propulsion performance. Appl Ocean Res 2020;94:102006. https://doi.org/10.1016/j.apor.2019.102006.
[6] International Energy Agency. Hydropower special market report. Paris: International Energy Agency; 2021.
[7] U.S. Energy Information Administration. International Energy Outlook 2016. Washington: U.S. Energy Information Administration; 2016.
[8] Han X, Wu JH, Zhang XH, Shi JY, Wei JX, Yang Y, et al. The progress on antifouling organic coating: From biocide to biomimetic surface. J Mater Sci Technol 2021;61:46–62. https://doi.org/10.1016/j.jmst.2020.07.002.
[9] Suleiman RK, Saleh TA, Al Hamouz OCS, Ibrahim MB, Sorour AA, El Ali B. Corrosion and fouling protection performance of biocide-embedded hybrid organosiloxane coatings on mild steel in a saline medium. Surf Coat Technol 2017;324:526–35. https://doi.org/10.1016/j.surfcoat.2017.06.028.
[10] Zhang J, Richardson MOW, Wilcox GD, Min J, Wang X. Assessment of resistance of non-metallic coatings to silt abrasion and cavitation erosion in a rotating disk test rig. Wear 1996;194(1–2):149–55. https://doi.org/10.1016/0043-1648(95)06823-6.
[11] Yamaguchi A, Wang X, Kazama T. Evaluation of erosion-resisting properties of plastics and metals using cavitating jet apparatus. SAE Trans 2002:186–93. https://doi.org/10.4271/2002-01-1386.
[12] Bohm H, Betz S, Ball A. The wear-resistance of polymers. Tribol Int 1990;23(6):399–406. https://doi.org/10.1016/0301-679x(90)90055-t.
[13] Hattori S, Itoh T. Cavitation erosion resistance of plastics. Wear 2011;271(7–8):1103–8. https://doi.org/10.1016/j.wear.2011.05.012.
[14] Deplancke T, Lame O, Cavaille JY, Fivel M, Riondet M, Franc JP. Outstanding cavitation erosion resistance of ultra high molecular weight polyethylene (UHMWPE) coatings. Wear 2015;328:301–8. https://doi.org/10.1016/j.wear.2015.01.077.
[15] Yilgor I, Yilgor E, Wilkes GL. Critical parameters in designing segmented polyurethanes and their effect on morphology and properties: A comprehensive review. Polymer 2015;58:A1–36. https://doi.org/10.1016/j.polymer.2014.12.014.
[16] Kontou E, Spathis G, Niaounakis M, Kefalas V. Physical and chemical cross-linking effects in polyurethane elastomers. Colloid Polym Sci 1990;268(7):636–44. https://doi.org/10.1007/bf01410405.
[17] Chattopadhyay DK, Raju K. Structural engineering of polyurethane coatings for high performance applications. Prog Polym Sci 2007;32(3):352–418. https://doi.org/10.1016/j.progpolymsci.2006.05.003.
[18] Zhang RZ, Ren YY, Yan DK, Guo PY, Li LJ. Synthesis of hydrophobic fluorinated polyurethanes and their properties of resistance to cavitation and wear. Prog Org Coat 2017;104:11–9. https://doi.org/10.1016/j.porgcoat.2016.12.002.
[19] Xie FW, Zhang TL, Bryant P, Kurusingal V, Colwell JM, Laycock B. Degradation and stabilization of polyurethane elastomers. Prog Polym Sci 2019;90:211–68. https://doi.org/10.1016/j.progpolymsci.2018.12.003.
[20] Yang HC, Zhang ML, Chen RR, Liu Q, Liu JY, Yu J, et al. Polyurethane coating with heterogeneity structure induced by microphase separation: A new combination of antifouling and cavitation erosion resistance. Prog Org Coat 2021;151:12106032. https://doi.org/10.1016/j.porgcoat.2020.106032.
[21] Qiao XN, Chen RR, Zhang HS, Liu JY, Liu Q, Yu J, et al. Outstanding cavitation erosion resistance of hydrophobic polydimethylsiloxane-based polyurethane coatings. J Appl Polym Sci 2019;136(25):1147668. https://doi.org/10.1002/app.47668.
[22] Luo G, Jin Z, Dong Y, Huang J, Zhang R, Wang J, et al. Preparation and performance enhancements of wear-resistant, transparent PU/SiO_2 superhydrophobic coating. Surf Eng 2018;34(2):139–45. https://doi.org/10.1080/02670844.2016.1236068.
[23] Hu LQ, Pu ZJ, Tian YH, Zheng XY, Cheng J, Zhong JC. Preparation and properties of fluorinated silicon two-component polyurethane hydrophobic coatings. Polym Int 2020;69(5):448–56. https://doi.org/10.1002/pi.5973.
[24] Wang X, Hu JJ, Li Y, Zhang JR, Ding YY. The surface properties and corrosion resistance of fluorinated polyurethane coatings. J Fluor Chem 2015;176:14–9. https://doi.org/10.1016/j.jfluchem.2015.04.002.
[25] Wang XY, Cui Y, Wang YN, Ban T, Zhang YY, Zhang JS, et al. Preparation and characteristics of crosslinked fluorinated acrylate modified waterborne polyurethane for metal protection coating. Prog Org Coat 2021;158:12106371. https://doi.org/10.1016/j.porgcoat.2021.106371.
[26] Wu ZJ, Tang LY, Dai JT, Qu JQ. Synthesis and properties of fluorinated non-isocyanate polyurethanes coatings with good hydrophobic and oleophobic properties. J Coat Technol Res 2019;16(5):1233–41. https://doi.org/10.1007/s11998-019-00195-5.
[27] Wang SJ, Liu WQ, Tan JQ. Synthesis and properties of fluorine-containing polyurethane based on long chain fluorinated polyacrylate. J Macromol Sci A 2016;53(1):41–8. https://doi.org/10.1080/10601325.2016.1110456.
[28] Li N, Zeng FL, Wang Y, Qu DZ, Hu WB, Luan YG, et al. Fluorinated polyurethane based on liquid fluorine elastomer (LFH) synthesis via two-step method: the critical value of thermal resistance and mechanical properties. RSC Adv 2017;7(49):30970–8. https://doi.org/10.1039/c7ra04509c.
[29] Li DH, Liao MY. Study on the dehydrofluorination of vinylidene fluoride (VDF) and hexafluoropropylene (HFP) copolymer. Polym Degrad Stab 2018;152:116–25. https://doi.org/10.1016/j.polymdegradstab.2018.04.008.
[30] Maclachlan JD. Fluorocarbon elastomers: a technical review. Polym-Plast Technol Eng 1978;11(1):41–53. https://doi.org/10.1080/03602557808067655.
[31] Ameduri B, Boutevin B, Kostov G. Fluoroelastomers: synthesis, properties and applications. Prog Polym Sci 2001;26(1):105–87. https://doi.org/10.1016/s0079-6700(00)00044-7.
[32] Li DH, Liao MY. Preparation of Telechelic Hydroxyl Low Molecular Weight Fluoropolymers. Key Eng Mater: Trans Tech Publ 2017:93–8.
[33] Flint EB, Suslick KS. The temperature of cavitation. Science 1991;253(5026):1397–9. https://doi.org/10.1126/science.253.5026.1397.
[34] Ye L, Zhu X, He Y, Wei X. Ultrasonic cavitation damage characteristics of materials and a prediction model of cavitation impact load based on size effect. Ultrason Sonochem 2020;66:105115. https://doi.org/10.1016/j.ultsonch.2020.105115.

[35] Li N, Tian Y, Yang R, Zhang HJ, Li H, Chen XY. Superhydrophobic surface on arc-sprayed aluminum coating via fluorinated polyurethane modification: preparation and application in corrosion protection. J Therm Spray Technol 1906-17;31. https://doi.org/10.1007/s11666-022-01410-3.
[36] Lu T, Chen Q. Shermo: A general code for calculating molecular thermochemistry properties. Comput Theor Chem 2021;1200:113249. https://doi.org/10.1016/j.comptc.2021.113249.
[37] Lu T, Chen F. Multiwfn: a multifunctional wavefunction analyzer. J Comput Chem 2012;33(5):580–92. https://doi.org/10.1002/jcc.22885.
[38] Li Y, Zhu ZQ, Wang X. Synthesis and thermal properties of organically modified palygorskite/fluorinated polyurethane nanocomposites. J Appl Polym Sci 2018;135(28):845460. https://doi.org/10.1002/app.45460.
[39] Babaie A, Rezaei M, Sofia RLM. Investigation of the effects of polycaprolactone molecular weight and graphene content on crystallinity, mechanical properties and shape memory behavior of polyurethane/graphene nanocomposites. J Mech Behav Biomed Mater 2019;96:53–68. https://doi.org/10.1016/j.jmbbm.2019.04.034.
[40] Liu T, Ye L. Synthesis and properties of fluorinated thermoplastic polyurethane elastomer. J Fluor Chem 2010;131(1):36–41. https://doi.org/10.1016/j.jfluchem.2009.09.018.
[41] Ding SS, Fang C, Wang XH, Wang ZG. Crystallization-driven microstructure changes during microphase separation for environment-friendly thermoplastic triblock copolymer elastomers. Polymer 2020;186:11121993. https://doi.org/10.1016/j.polymer.2019.121993.
[42] Chang RX, Shan GR, Bao YZ, Pan PJ. Enhancement of crystallizability and control of mechanical and shape-memory properties for amorphous enantiopure supramolecular copolymers via stereocomplexation. Macromolecules 2015;48(21):7872–81. https://doi.org/10.1021/acs.macromol.5b01986.
[43] Banerjee I, Pangule RC, Kane RS. Antifouling coatings: recent developments in the design of surfaces that prevent fouling by proteins, bacteria, and marine organisms. Adv Mater 2011;23(6):690–718. https://doi.org/10.1002/adma.201001215.
[44] Yan W, Liu HT, Zhu W. Preparation of anti-corrosion superhydrophobic coatings by an Fe-based micro/nano composite electro-brush plating and blackening process. RSC Adv 2015;5(125):103000–12. https://doi.org/10.1039/c5ra15640h.
[45] Cengiz U, Erbil HY. Superhydrophobic perfluoropolymer surfaces having heterogeneous roughness created by dip-coating from solutions containing a nonsolvent. Appl Surf Sci 2014;292:591–7. https://doi.org/10.1016/j.apsusc.2013.12.013.
[46] Wang JL, Raza A, Si Y, Cui LX, Ge JF, Ding B, et al. Synthesis of superamphiphobic breathable membranes utilizing SiO_2 nanoparticles decorated fluorinated polyurethane nanofibers. Nanoscale 2012;4(23):7549–56. https://doi.org/10.1039/c2nr32883f.
[47] Ying WB, Yu Z, Kim DH, Lee KJ, Hu H, Liu YW, et al. Waterproof, highly tough, and fast self-healing polyurethane for durable electronic skin. ACS Appl Mater Interfaces 2020;12(9):11072–83. https://doi.org/10.1021/acsami.0c00443.
[48] Herrera M, Matuschek G, Kettrup A. Thermal degradation of thermoplastic polyurethane elastomers (TPU) based on MDI. Polym Degrad Stab 2002;78(2):323–31. https://doi.org/10.1016/s0141-3910(02)00181-7.
[49] Zhang Y, Shang S, Zhang X, Wang D, Hourston DJ. Influence of the composition of rosin-based rigid polyurethane foams on their thermal stability. J Appl Polym Sci 1996;59(7):1167–71. https://doi.org/10.1002/(sici)1097-4628(19960214)59:7<1167::Aid-app14>3.0.Co;2-2.
[50] Schick C. Differential scanning calorimetry (DSC) of semicrystalline polymers. Anal Bioanal Chem 2009;395(6):1589–611. https://doi.org/10.1007/s00216-009-3169-y.
[51] Xu W, Zhao WJ, Hao LF, Wang S, Pei MM, Wang XC. Synthesis and characterization of novel fluoroalkyl-terminated hyperbranched polyurethane latex. Appl Surf Sci 2018;436:1104–12. https://doi.org/10.1016/j.apsusc.2017.12.148.
[52] Abramowitz R, Yalkowsky SH. Melting point, boiling point, and symmetry. Pharm Res 1990;7(9):942–7. https://doi.org/10.1023/a:1015949907825.
[53] Chen KP, Tian CR, Lu A, Zhou QM, Jia XR, Wang JH. Effect of SiO_2 on rheology, morphology, thermal, and mechanical properties of high thermal stable epoxy foam. J Appl Polym Sci 2014;131(7):740068. https://doi.org/10.1002/app.40068.
[54] Shen JS, Shao ZZ, Li SJ. Physical aging studies of polysiloxane-modified epoxy-resin. Polymer 1995;36(18):3479–83. https://doi.org/10.1016/0032-3861(95)92019-b.
[55] Wetton RE, Marsh RDL, Vandevelde JG. Theory and application of dynamic mechanical thermal analysis. Thermochim Acta 1991;175(1):1–11. https://doi.org/10.1016/0040-6031(91)80240-j.
[56] Zhu JT, Wu ZM, Xiong D, Pan LS, Liu YJ. Preparation and properties of a novel low crystallinity cross-linked network waterborne polyurethane for water-based ink. Prog Org Coat 2019;133:161–8. https://doi.org/10.1016/j.porgcoat.2019.04.033.
[57] Yang R, Chen X, Tian Y, Chen H, Boshkov N, Li H. An attempt to improve cavitation erosion resistance of UHMWPE coatings through enhancing thermal conductivity via the incorporation of copper frames. Surf Coat Technol 2021;425:127705. https://doi.org/10.1016/j.surfcoat.2021.127705.
[58] Yoon J, Sim S, Myint AA, Lee YW. Kinetics of the hydrolysis of xylan based on ether bond cleavage in subcritical water. J Supercrit Fluids 2018;135:145–51. https://doi.org/10.1016/j.supflu.2018.01.013.
[59] Saha S, Sarkar P. Tuning the HOMO-LUMO gap of SiC quantum dots by surface functionalization. Chem Phys Lett 2012;536:118–22. https://doi.org/10.1016/j.cplett.2012.03.107.
[60] Buvaneswari M, Santhakumari R, Usha C, Jayasree R, Sagadevan S. Synthesis, growth, structural, spectroscopic, optical, thermal, DFT, HOMO-LUMO, MEP, NBO analysis and thermodynamic properties of vanillin isonicotinic hydrazide single crystal. J Mol Struct 2021;1243:11130856. https://doi.org/10.1016/j.molstruc.2021.130856.
[61] Fujita N, Yamaguchi H, Kinoshita T, Iwao M, Nakanishi Y. Friction behaviors of elastic materials sliding on textured glass surfaces. Tribol Int 2022;171:15107539. https://doi.org/10.1016/j.triboint.2022.107539.